Effects of the pannexin-1 hemichannel inhibitor probenecid on rat enteric glial cells following intestinal ischemia and reperfusion

Cristina Eusébio Mendes
Uninove: Universidade Nove de Julho
Kelly Palombit
Federal University of Piaui: Universidade Federal do Piaui
Thaira Thalita Alves Pereira
University of Sao Paulo: Universidade de Sao Paulo
Patricia Castelucci (pcastel@usp.br)
University of São Paulo https://orcid.org/0000-0002-7475-5962

Research Article

Keywords: Myenteric Plexus, Ileum, Enteric Glial Cell, Probenecid, Pannexin-1 Channel

Posted Date: March 3rd, 2022

DOI: https://doi.org/10.21203/rs.3.rs-1352811/v1

Abstract

Background : This study examined the effects of probenecid (PB), a pannexin-1 channel antagonist, on the enteric glial cells of the rat ileum after ischemia and reperfusion.

Methods: The ileal vessels were occluded for 45 min with atraumatic vascular clamps, and the tissue was then reperfused for periods of 24 h and 14 and 28 days. After ischemia, the animals were either left without further treatment (IR groups) or treated with PB (PB groups).

Results: The results demonstrated that glial cells were immunoreactive for S100β and/or GFAP and that the pannexin-1 channel was present in glial cells. Density analyses (in cells/cm^2) showed that the IR groups exhibited a decrease in the numbers of cells immunoreactive for pannexin-1 and HuC/D and that treatment with PB caused their numbers to recover. The number of glial cells (S100β and GFAP) was elevated in the IR group, and PB treatment decreased the total number of glia, but the number of S100β-positive glia did not recover. Additionally, the cell profile area (μm^2) of S100β-positive glial cells showed no recovery in the PB groups. The contractile activity of the ileum was decreased in the IR groups and restored in the PB groups.

Conclusions: PB can effectively induce the recovery of neurons and glial cells and is thus a potential therapeutic agent for diseases of the gastrointestinal tract.

Background

Enteric glial cells (EGCs) are small, star-shaped, non-myelin-synthesizing cells that have numerous branches and processes and intermingle with neurons and bundles of axons; EGCs express several varieties of neurotransmitter receptors, such as purinergic receptors, adrenergic receptors, and metabotropic glutamate receptors [1–3]. EGCs support neurons, regulate synaptic transmission [4], mediate communication between the nervous and immune systems [4], create a protective microenvironment [3] and regulate the intestinal barrier [5, 6]. The markers that have been used to identify EGCs include glial acid fibrillar protein (GFAP) and S100/S100β calcium-binding protein [7, 8]. EGCs are found in circular and longitudinal muscles [9] and are distributed throughout the enteric nervous system (ENS) [10].

Pannexin channels are families of membrane proteins (pannexin-1, 2 and 3) that are expressed in both vertebrates and invertebrates and exhibit sequential homology of approximately 20% with innexins that form gap junctions; however, pannexin channels do not form gap junctions [11–13]. Pannexin-1 channels are nonselective and form large pores in the plasma membrane [11, 14]. The opening of pannexin channels allows the release of molecules, such as ATP and other metabolites that are important for cell communication and autocrine/paracrine signaling, into the extracellular medium [15–17]. Additionally, pannexin-1 has been found to be involved in the release of ATP in models of inflammation [18]. Extracellular ATP can activate the P2X7 receptor, which activates an inflammatory response in immune cells involving the release of cytokines such as IL-1b [19]. Diezmos et al. (2013) [20] showed that the

pannexin-1 channel is present in all layers of the human large intestine and that the expression of this protein is decreased in the muscle of the colon in individuals with Crohn's disease.

Researchers have shown that probenecid decreases the luminance dye uptake of oocytes expressing pannexin, which indicates that probenecid can be used as a pannexin channel antagonist [21]. Mice without pannexin-1 and pannexin-2 channels exhibited a reduced infarction size after cerebral ischemia and improved neurological evolution [22]. Additionally, other researchers have explored ischemia of the carotid artery and found that the injection of probenecid resulted in a decrease in the injury score and recovery of neuronal density [23].

Intestinal ischemia is a life-threatening abdominal emergency, and its prognosis depends on rapid diagnosis, which allows the timely administration of treatment to prevent substantial bowel infarction. The associated mortality rate has remained high over the last decade, varying between 60% and 80%, and its incidence has considerably increased [24].

The Cx43 hemichannel has been shown to mediate calcium responses in EGCs and modulate colonic transit in mice [25, 26]. Pannexin channels appear to regulate the control of motility, secretion, and blood flow [25, 26]. ATP could play an excitatory transmitter role in EGCs in maintaining cholinergic excitability in postinflammatory ileitis [27]. Activation of the pannexin-1 channel in neuronal death and as a consequence of dysmotility in inflammatory bowel disease (IBD) has been described [28]. Additionally, changes in the distribution of the pannexin-1 channel in the colon of patients with IBD have been demonstrated [20].

Due to the high mortality rate among patients suffering from intestinal impairment who are hospitalized in wards and intensive care units, an experimental model of ischemia and reperfusion has clinical importance. In addition, understanding the role of enteric glia in this process and clarifying the interactions of the pannexin-1 channel using probenecid might be extremely important for developing drugs and therapeutic strategies for gastrointestinal disorders caused by intestinal ischemia and reperfusion. This work aimed to study the effects of intestinal ischemia and reperfusion on EGCs and enteric neurons expressing pannexin-1 channels, as well as intestinal motility, and to assess the influence of the pannexin-1 channel antagonist PB.

Methods

Young male Wistar rats were obtained from the Central Animals House (Bioterium) of the Institute of Biomedical Sciences of the University of São Paulo. The animal experiments in this study were conducted according to the current regulations of the Ethics Committee on Animal Use of the Biomedical Science Institute of the University of São Paulo. Furthermore, all the protocols were approved by the Ethics Committee on Animal Use of the Biomedical Science Institute of the University of São Paulo (Protocol 126/2016). Young male Wistar rats (with a body weight of 200–300 g) were maintained under standard conditions at 21°C and a 12/12-h light-dark cycle. All the groups were supplied with water *ad libitum*.

Induction of Ischemia

A total of 45 rats were anesthetized with a subcutaneously administered mixture of xylazine (20 mg/kg) and ketamine hydrochloride (100 mg/kg). A loop of the distal ileum was exposed, and the ileal artery was located and occluded for 45 min with an atraumatic microsurgical vascular clamp (Vascu-statt) (IR group). Intestinal reperfusion was established by releasing the clamp [29–31]. The 15 rats that composed the sham groups were subjected to identical manipulations, but without arterial occlusion. Probenecid (PB, 10 mg/kg, Sigma Aldrich, United Kingdom) or saline was injected 1 h following reperfusion for the rats in the 24-h, 14-day and 28-day groups and once daily for 5 days after ischemia for the rats in the 14-day and 28-day groups [23]. PB and saline were administered subcutaneously. Twenty four h, 14 days and 28 days, animals were weighed, euthanized in a CO_2 chamber, and the anterior abdominal wall was opened. The ileum was removed and washed in phosphate-buffered saline (PBS; 0.15 M NaCl in 0.01 M sodium phosphate buffer, pH 7.2). Five rat ilea from the IR group, five rat ilea from the IR group treated with probenecid (PB) and five rat ilea from the sham-operated group (Sh group) were used for immunofluorescence analysis. The following 9 groups were included in this study: 24h-Sh, 24h-IR, 24h-PB, 14d-Sh, 14d-IR, 14d-PB, 28d-Sh, 28d-IR, and 28d-PB (n = 5 animals per group).

Immunohistochemistry

Forty-five ileal segments were dissected for immunohistochemistry, cleaned with PBS, pinned mucosal side down onto a balsa wood board and fixed overnight at 4°C with 4% paraformaldehyde in 0.2 M sodium phosphate buffer (pH 7.3). Tissue collection was performed by the same researcher to maintain the same degree of tension in all preparations. The tissue was then subjected to three 10-min washes in 100% dimethyl sulfoxide (DMSO, Sigma Aldrich, United Kingdom), followed by three 10-min washes in PBS. The tissue was subsequently stored at 4°C in PBS containing sodium azide (0.1%). Prior to use, the tissue was dissected to prepare whole-mount longitudinal muscle–myenteric plexus preparations. Segments from five rats per group were used. A total of 2 whole-mount preparations per animal were used in each double labeling. The tissues were incubated in 10% normal horse serum in PBS containing 1.5% Triton X-100 (Amresco) for 45 min at room temperature to reduce nonspecific binding and permeabilize the tissue. The antibodies and antibody combinations used for double labeling are described in Table 1. Following incubation in the primary antisera for 48 h at 4°C using the free-floating method, the tissue was subjected to three 10-min washes in PBS and incubated with various secondary antibodies for 1 h at room temperature using the free-floating method (Table 1). The PBS washes were repeated, and the tissue was mounted in glycerol buffered with 0.5 M sodium carbonate (pH 8.6). The preparations were examined with a Nikon 80i (Tokyo, Japan) fluorescence microscope, and images were captured using a digital camera and Image-Pro Plus software version 4.1.0.0. Additionally, the preparations were analyzed by confocal microscopy using a Zeiss confocal scanning laser system installed on a Zeiss Axioplan 2 microscope (Zeiss, Oberkochen, Germany). Confocal images were collected using Zeiss LSM 5 image-processing software and further processed using Corel Draw software. Negative control experiments for the pannexin-1 channel were performed, and no receptor or channel staining was observed.

Table 1
Characteristics of primary and secondary antibodies.

Antigen	Host	Dilution	Source	Identification code
Pannexin-1 channel	Goat	1:100	Santa Cruz	sc-49695/Lot n°. F2413
Pannexin-1 channel	Rabbit	1:100	Life Tech Novex	488000/Lot n°. QJ224111
GFAP	Rabbit	1: 400	Dako	Z0334/Lot n°. 00061481
GFAP	Mouse	1:200	Sigma	G3893/Lot n°. 032M4779
S100β	Mouse	1:300	Millipore	MAB079-1/Lot n°. NMM1724156
S100β	Rabbit	1:400	Dako	Z0311/Lot n°. 00040840
HuC/D	Mouse	1:200	Molecular Probes	A21271/Lot n°. 43471A
Secondary antibodies				
Donkey anti-rabbit IgG 488		1:500	Molecular Probes	A21206/Lot n°. 1182675
Donkey anti-mouse IgG 594		1:200	Molecular Probes	A21203/Lot n°. 93E-1
Goat anti-mouse IgG 488		1:200	Molecular Probes	A11029/Lot n°. 419251
Donkey anti-goat IgG 594		1:100	Molecular Probes	A11058/Lot n°. 1608643

Quantitative Analyses

For the colocalization studies, neurons were identified by immunofluorescence. The labeling of the second antigen was evaluated using a second filter, which allowed calculation of the proportion of neurons labeled with the antigen pairs. For each group, the data were collected from two preparations obtained from five animals and from 100 neurons per animal. The percentages of double-positive neurons were calculated and are expressed as the means ± standard errors of the mean (SEMs). The density values (neurons/cm^2) of neurons immunoreactive for the pannexin-1 channel and pan-neuronal HuC/D and the density values (glial cells/cm^2) of EGCs immunoreactive for GFAP and S100β were measured using two whole-mount preparations from five rats in each group [25, 26]. For each antigen, counts were obtained from 40 microscopic fields (0.000379 cm^2) selected at random from each animal, and a total of 200 microscopic fields were analyzed for each type of immunoreactivity [25, 26]. The cell profile areas (μm^2) were obtained from 100 randomly selected neurons in two whole-mount preparations per animal; five animals in each group were used in each immunoreactivity test, and thus, a total of 500 neurons per group were analyzed using a Nikon 80i microscope coupled to a camera with NIS-Elements AR 3.1 (Nikon) software and were measured using Image-Pro Plus software version 4.1.0.0 [25, 26]. The quantitative analyses were conducted in an unblinded manner.

Intestinal Motility

A total of 36 rats were used in the analysis of intestinal motility; the animals were divided into the following 9 groups: 24h-Sh, 24h-IR, 24h-PB, 14d-Sh, 14d-IR, 14d-PB, 28d-Sh, 28d-IR, and 28d-PB (n = 4 animals per group). Full-thickness ileal segments (2 cm long) were used. Segments from four rats in each group were prepared and mounted longitudinally in 20-ml organ baths containing Krebs' physiological saline solution with the following composition (in mmol/l): 118 NaCl, 4.8 KCl, 2.5 $NaHCO_3$, 25 NaH_2PO_4, 1.1 $MgSO_4$, 11.1 D-glucose, 2.5 $CaCl_2$. The baths were aerated with 95% O_2/5% CO_2 and maintained at 37°C. A resting tension of 1 g was applied to the tissues, and isometric responses were recorded with a force transducer and displayed using AcqKnowledge 4 software (BIOPAC Systems, Inc., USA). The tissues were allowed to equilibrate for at least 60 min before the experiments, and amplitude–response curves were obtained before, during, and after the addition of carbachol (0.01 μM, 0.1 μM, 1.0 μM, 10 μM and 100 μM; Sigma Aldrich). In addition, contractile responses were elicited by electrical field stimulation delivered at 5, 10 and 20 Hz (0.5-ms pulse width, 100 pulses, 60 V). Before the experiments were started, the viability of each preparation was confirmed by testing its contractile response to acetylcholine [29, 31].

Statistical Analyses

The data were compared by analysis of variance (ANOVA) and Tukey's multiple comparison test. The data are reported as the means ± SEMs, and $P < 0.05$ was considered to indicate statistical significance. We used GraphPad Prism 5 (GraphPad Software, USA, v5) to analyze the data.

Results

The preparations were examined with a Nikon 80i fluorescence microscope and by confocal microscopy using a Zeiss confocal scanning laser system installed on a Zeiss Axioplan 2 microscope.

The double labeling of S100β/GFAP is shown in Fig. 1. In this analysis, EGCs that were immunoreactive for both GFAP and S100β, for GFAP alone, or for S100β alone were observed. EGCs that were immunoreactive for GFAP showed filamentous labeling patterns with many branches (Fig. 1, 24h and 14 days groups; Fig. 3, 28 days group). In general, the quantitative analysis of the double labeling in all the groups revealed that GFAP+/S100β + and GFAP+/S100β- EGCs accounted for 69.5 ± 1.4% and 30.5 ± 1.4% of EGCs, respectively. In addition, 71 ± 2% of EGCs exhibited positive S100β and GFAP staining, and 29 ± 2% of EGCs showed positive S100β staining and negative GFAP staining (for more details, see Table 2).

Table 2
Percentages of EGCs immunoreactive for GFAP and S100β.

Groups	GFAP+/S100β+	GFAP+/S100β-	S100β+/GFAP+	S100β-/GFAP+
24h-Sh	70 ± 0.7	30 ± 0.7	72 ± 1.8	28 ± 1.8
24h-IR	70.6 ± 0.8	29.4 ± 0.8	69.8 ± 0.8	30.2 ± 0.8
24h-PB	70.5 ± 0.6	29.5 ± 0.6	70.7 ± 0.9	29.2 ± 0.9
Mean	70.5 ± 0.8	29.5 ± 0.8	70.9 ± 1.1	29.0 ± 1.1
14d-Sh	69.2 ± 1.3	30.8 ± 1.3	70.1 ± 0.9	29.9 ± 0.9
14d-IR	68.4 ± 0.9	31.6 ± 0.9	72.5 ± 1.5	27.5 ± 1.5
14d-PB	70 ± 0.8	30 ± 0.8	70.7 ± 1.5	29.2 ± 1.5
Mean	69.5 ± 1.2	30.5 ± 1.2	71 ± 1.5	28.9 ± 1.5
28d-Sh	69 ± 0.7	31 ± 0.7	72.2 ± 2	27.8 ± 2
28d-IR	69 ± 1	31 ± 1	70 ± 0.7	30 ± 0.7
28d-PB	69 ± 0.8	31 ± 0.8	69.3 ± 0.9	30.7 ± 0.9
Mean	69.0 ± 0.8	31 ± 0.8	70.5 ± 1.2	29.4 ± 1.2
The data are expressed as the means ± SEMs; n = 5 per group				

Qualitatively, double labeling of pannexin-1 and GFAP in EGCs was observed in the myenteric ganglia of the rats in all the groups (Fig. 2, 24h and 14 days groups; Fig. 3, 28 days group). Quantitative double-labeling analyses showed 100% colocalization of GFAP and pannexin-1 staining in EGCs. Figure 4 shows HuC/D-positive neurons in the myenteric ganglia of the rats in all the groups.

Quantitative Analyses

To test the effects of PB treatment on neurons and EGCs, the number and area of cells positive for pannexin-1 channels, EGCs positive for GFAP and S100β and neurons positive for HuC/D were assessed.

The cells immunoreactive for pannexin-1 channel per unit area (cm^2) showed decreases of 18 ± 0.7%, 9 ± 0.3% and 6 ± 0.5% ($P < 0.05$) in the 24-h, 14-day and 28-day IR groups, respectively, compared with the corresponding Sh groups. The PB groups (24 h, 23 ± 0.7%; 14 days, 8 ± 0.01%; and 28 days, 6 ± 0.6%) showed increases ($P < 0.05$) compared with the corresponding IR groups (Fig. 5A).

The density (GFAP/cm^2) of glial cells immunoreactive for GFAP in the 24-h, 14-day and 28-day IR groups showed increases of 13 ± 0.4%, 38 ± 0.3% and 14 ± 0.1% ($P < 0.05$), respectively, compared with the levels in the respective Sh groups. The PB groups presented significant decreases at 24 h (9 ± 0.6%), 14 days (21 ± 0.7%), and 28 days (9 ± 0.4%) ($P < 0.05$) compared with the corresponding IR groups (Fig. 5B).

The density of S100β per square centimeter in the 24-h, 14-day and 28-day IR groups was increased by 14 ± 0.1%, 13 ± 0.3%, and 12 ± 0.3 ($P < 0.05$), respectively, compared with the corresponding Sh groups. The 24-h, 14-day and 28-day PB groups showed decreases of 57 ± 0.1%, 41 ± 0.2%, and 45 ± 0.6% ($P < 0.05$), respectively, compared with the corresponding IR groups (Fig. 5C).

The density of HuC/D-immunoreactive neurons (neurons/cm^2) in the 24-h, 14-day and 28-day IR groups showed decreases of 17 ± 0.3%, 18 ± 0.1%, and 25 ± 0.3% ($P < 0.05$), respectively, compared with the corresponding Sh groups. The PB groups presented increases in this variable at 24 h (11 ± 0.6%), 14 days (9 ± 0.4%), and 28 days (8 ± 0.7%) ($P < 0.05$) compared with the respective IR groups (Fig. 5D).

Ischemia affects the area of neurons and glial cells; thus, their area was measured after the different treatments.

The analysis of the profile area (μm^2) of neurons immunoreactive for HuC/D revealed a significant but small increase ($P < 0.05$) of only 8 ± 0.4% in the 24h-PB group compared with the 24h-IR group, and no significant differences were found among the other groups (Fig. 6A).

The analysis of the profile area (μm^2) of EGCs positive for S100β revealed a decrease of 45 ± 0.7% in the 24h-IR group compared with the corresponding Sh group ($P < 0.05$). The profile area in the 24h-PB group was increased by 50 ± 0.4% compared with that in the 24h-IR group ($P < 0.05$) (Fig. 6B). The 14d-IR group exhibited a decrease of 35 ± 0.3% ($P < 0.05$) compared with the corresponding Sh group, and the 14d-PB group presented an increase of 23 ± 0.1% ($P < 0.05$) compared with the 14d-IR group (Fig. 6B). The 28d-IR group showed a decrease of 26 ± 0.1% compared with the corresponding Sh group ($P < 0.05$), and the 28d-PB group showed an increase of 19 ± 0.3% ($P < 0.05$) compared with the 28d-IR group (Fig. 6B).

Myographic Recordings of Contractile Activity

PB treatment resulted in the recovery of enteric neurons and glia positive for GFAP after the ischemia and reperfusion protocol, and experiments were thus performed to verify the recovery of intestinal motility.

The analysis of spontaneous activity showed decreases of 6.1 ± 0.1%, 5.1 ± 0.01%, and 10 ± 0.2% in the 24h-IR, 14d-IR and 28d-IR groups compared with the 24h-Sh, 14d-Sh and 28d-Sh groups ($P < 0.05$), respectively. No significant difference was found among the Sh, 14d-PB and 28d-PB groups or between the 24h-IR and 24h-PB groups (Fig. 7).

The contractions induced after the application of carbachol at concentrations of 1.0 μM, 10.0 μM and 100 μM were lower by 82.5 ± 0.8%, 82.5 ± 0.6% and 80 ± 0.4%, respectively, in the 24h-IR group than in the 24h-Sh group ($P < 0.05$). In addition, increases of 20.3 ± 0.9% and 80.5 ± 0.3% were detected in the 24h-PB group compared with the 24h-IR group at concentrations of 10.0 μM and 100 μM, respectively ($P < 0.05$) (Fig. 8A).

Among the 14-day groups, the contractions induced after the application of carbachol at concentrations of 1.0 μM, 10.0 μM and 100 μM showed decreases of 49.2 ± 0.5%, 49.1 ± 0.6% and 35.5 ± 0.1%,

respectively, in the 14d-IR group compared with the 14h-Sh group ($P < 0.05$). The application of carbachol at concentrations of 10 μM and 100 μM induced more contractions (by 39.7 ± 1% and 49 ± 0.7%, respectively; $P < 0.05$) in the 14d-PB group than in the 14d-IR group. No significant differences were found between the 14d-Sh and 14d-PB groups (Fig. 8B).

The analysis of the 28-day groups revealed that the contractions induced after the application of carbachol at concentrations of 1.0 μM, 10.0 μM and 100 μM, respectively, were 67.4 ± 0.9%, 42.4 ± 0.7% and 33.7 ± 0.4% lower in the 28d-IR group than in the 28d-Sh group ($P < 0.05$). Increases of 16.4 ± 1% (10.0 μM) and 23.9 ± 0.01% (100 μM) were found in the 28d-PB group compared with the 28d-IR group ($P < 0.05$). No significant differences were detected between the 14d-Sh and 14d-PB groups (Fig. 8C).

The analysis of the contraction amplitude after simulation with 5-Hz, 10-Hz and 20-Hz electrical fields demonstrated significant decreases of 64.4 ± 0.2%, 62.8 ± 0.4% and 52.6 ± 0.7%, respectively, in the 24h-IR group compared with the 24h-Sh group ($P < 0.05$). No significant differences were found among the 24h-Sh, 24h-PB and 24h-IR groups (Fig. 9A).

The contraction amplitude after stimulation with an electrical field at 5 Hz, 10 Hz and 20 Hz was lower by 79.9 ± 0.2%, 80.9 ± 0.3%, and 66.4 ± 0.7%, respectively, in the 14d-IR group than in the 14d-Sh group ($P < 0.05$). The contraction amplitude detected in the 14d-PB group after stimulation with 5 Hz and 10 Hz was higher than that in the 14d-IR group by 63.9 ± 0.2% and 57.2 ± 0.7%, respectively ($P < 0.05$). No significant differences were detected between the 14d-Sh and 14d-PB groups after stimulation with 10 Hz and 20 Hz (Fig. 9B).

The analysis of the 28-day groups showed that the contraction amplitude after stimulation with an electrical field at 5 Hz, 10 Hz and 20 Hz, respectively, was 77.3 ± 0.7%, 74.8 ± 0.6% and 60 ± 0.7% lower in the 28d-IR group than in the 28d-Sh group ($P < 0.05$). The contraction amplitudes observed in the 28d-PB group after stimulation with 5 Hz and 10 Hz, respectively, were 45.7 ± 0.1% and 29.4 ± 0.3% higher than those in the 28d-IR group ($P < 0.05$). No significant differences in the contraction amplitude were found between 28d-Sh and 28d-PB after stimulation with 10 Hz and 20 Hz (Fig. 9C).

Discussion

Through immunohistochemistry and intestinal motility analyses, this study demonstrated the effects of PB treatment on EGCs subjected to different periods of ischemia and reperfusion. PB treatment induced the recovery of GFAP-positive EGCs. However, treatment with PB did not result in the recovery of S100β-positive EGCs positive. Neurons positive for HuC/D showed recovery after treatment with PB. The analysis of intestinal motility showed that PB was effective. We visually confirmed that our 45-min ileal vessel clamping technique efficiently induced ischemia, in that the intestine became purple in color during vessel clamping and regained its normal color after the removal of the clamp, as has been previously described [29–32]. The use of immunohistochemistry to identify EGCs using GFAP or S100β as a marker was efficient and demonstrated the presence of two different glial cell phenotypes [33]. The antibodies used in this work were effective for the identification of enteric neurons and pannexin-1 channels. The

organ bath method was very useful for studying intestinal motility after treatment with PB and the application of carbachol and electrical stimuli. Additionally, the use of the antagonist PB did not cause harmful functional changes in the animals studied.

Regarding the pannexin-1 channel, this study found that this channel was present in 100% of EGCs. In the presence of injury or pathological conditions, the pannexin-1 channel can open and thus allow the release of intracellular ATP into the extracellular environment, and this action can further aggravate the inflammatory process [33–35].

In the present study, double labeling of GFAP and S100β was performed to study the phenotype of EGCs. The results demonstrated that in all the groups studied, 70% of EGCs showed GFAP/S100β colocalization, and 29% of EGCs were immunoreactive for only S100β or GFAP. Previous studies have demonstrated the phenotypic heterogeneity of EGCs, and the differential expression of S100 and GFAP in these cells indicates their high plasticity [36–38]. Boesman et al. (2014) [36] morphologically classified EGCs into types I, II and III and then performed experiments to assess the colocalization of GFAP and S100β. Among type I EGCs, 55.8 ± 5.2% were GFAP+/S100β+, whereas GFAP-/S100β + and GFAP+/S100β- cells accounted for 29.9 ± 4.4% and 14.3 ± 3.9%, respectively. Among type II EGCs, the percentage of GFAP-/S100β + cells was 59.6 ± 1.6%; among type III EGCs, the percentage of GFAP-/S100β + cells was 78.9 ± 0.7%. Grundmann et al. (2016) [37] also showed colabeling of S100β and GFAP.

Ischemia–reperfusion injury reduces the numbers of enteric neurons and EGCs expressing HuC/D and S100β, respectively, per unit area [29, 30]. In the present study, treatment with the antagonist PB resulted in the recovery of HuC/D staining (pan-neuronal). Additionally, the use of PB has been shown to exert protective effects against oxygen and glucose deprivation injuries by regulating inflammatory activity [39]. Wei et al. (2015) [23] showed that PB has a neuroprotective effect against brain ischemia and reperfusion injuries, and another study also found that PB suppresses inflammatory processes and reduces the release of high-mobility group box 1 protein (a proinflammatory cytokine) in neurons after cerebral ischemia [40].

The analysis of EGCs per unit area revealed that this variable increased in the various IR groups. The increase in EGCs positive for GFAP and S100β in the present study could be explained by the neuroprotective action of EGCs after injury to the ENS [29–30]. Previous studies have reported the importance of EGCs in the biology and function of enteric neurons as well as in neurochemical coding, the release and degradation of neuroactive substances, and neuroprotection; all of these mechanisms have been shown to be modulated by EGCs [1–3].

In our study, we observed that treatment with PB exerted different effects on GFAP-immunoreactive and S100β-immunoreactive cells. The treatment of GFAP-positive cells with PB has been shown to be effective, and the effects are similar to those obtained after treatment with Brilliant Blue G (BBG) [31]. However, a marked decrease in S100β-positive cells was found in the PB-treated groups compared with

the other groups. S100 is implicated in the regulation of Ca^{2+} and has been reported to act as a Ca^{2+} sensor [41, 42]. Other previous studies have shown that intracellular Ca^{2+} is translocated to the extracellular fluid via pannexin channels [43]. Additionally, Ca^{2+} enters the cell from the extracellular fluid, and the increase in intracellular Ca^{2+} stimulates the opening of pannexin channels to release Ca^{2+} [33]. PB is known to directly reduce Ca^{2+} overload [23].

In addition, several studies have demonstrated that P2X7 and pannexin-1 receptors can act synergistically [9, 18, 28, 33] and that they are associated with the same harmful signaling cascade that leads to neuronal and tissue death [44]. Another study showed that PB also exerts a direct effect as an inhibitor of the P2X7 receptor [45]. Additionally, Gulbransen et al. (2012) [28] administered PB to mice with intestinal inflammation and observed a recovery of enteric neurons. Extracellular ATP can activate the P2X7 receptor, which stimulates an inflammatory response in immune cells, such as the release of IL-1b and other cytokines [19].

In the present study, the profile area of neurons positive for HuC/D was assessed. The results revealed a wide variety of neuron sizes, ranging from small to medium and large, among the groups analyzed, and no difference was detected between the groups. However, Palombit et al. (2019) [31] observed different results because different classes of neurons are analyzed using different ischemia protocols, and an increase or decrease in the positive area can be detected depending on whether nNOS, ChAT or NF-200 positivity as assessed. For EGCs specifically, the profile area was reduced in the IR groups and restored in the PB groups.

In the present study, decreases in spontaneous activity, activity after the application of carbachol, and contraction amplitude after electrical field stimulation were observed in the IR groups. Regarding the contractile activity of the intestine, some studies suggest that intrinsic neural circuits might be impaired as a result of ischemia–reperfusion injury; some neurons might die, and others might change after injury [25, 27, 32, 46]. Additionally, ATP causes the death of enteric neurons and changes in intestinal motility during P2X7 receptor–dependent intestinal inflammation, which affects glia, neurons and the expression of connexin-42 [47].

The PB groups, particularly the 24h-PB group, did not respond to low carbachol concentrations or electrical field stimulation at 5 Hz, 10 Hz or 20 Hz. Contraction amplitudes were observed to recover after the application of low concentrations of carbachol and electrical field stimulation in the 14-day and 28-day PB groups. ATP exits through the pannexin channel into the extracellular fluid [28, 48] and exerts autocrine and paracrine effects on the P2X7 receptor [19]. Additionally, fast excitatory synaptic potentials (EPSPs) have been shown to participate in P2X receptor activity [49, 50]. It has been reported that a decrease in the number of EGCs can result in disturbances in intestinal motility [51, 52].

Conclusions

The importance of this study is that it demonstrated the effects of ischemia followed by different periods of reperfusion on EGCs immunoreactive for S100β and GFAP. In addition, this study revealed that PB can effectively induce the recovery of GFAP-positive EGCs and neurons and could thus be a therapeutic agent for diseases of the gastrointestinal tract.

Abbreviations

PB
probenecid
IR
ischemia and reperfusion
Sh group
sham-operated group
GFAP
glial acid fibrillar protein
EGCs
Enteric glial cells
ENS
enteric nervous system
ATP
Adenosine 5’-triphosphate
PBS
phosphate-buffered saline
DMSO
dimethyl sulfoxide
CONCEA
National Council for Control and Animal Experimentation

Declarations

Ethics approval and consent to participate

The animal experiments in this study were conducted according to the current regulations of the Ethics Committee on Animal Use of the Biomedical Science Institute of the University of São Paulo. Furthermore, all the protocols were approved by the Ethics Committee on Animal Use of the Biomedical Science Institute of the University of São Paulo (Protocol 126/2016). This study, conducted for scientific research purposes, is in accordance with provisions of Law n° 11.794 (passed October 8th, 2008), Decree n° 6899 (passed on July 15th, 2009), and the rules issued by the National Council for Control and Animal Experimentation (CONCEA). According to this legislation, the project was evaluated and approved on 12/19/2016 by the Ethics Committee on Animal Use, Institute of Biomedical Sciences, University of São Paulo (CEUA-ICB/SP).

Consent to publish

Not applicable

Availability of data and materials

The datasets used and/or analysed during the current study are available from the corresponding author on reasonable request.

Competing interests

On behalf of all authors, the corresponding author states that there is no conflict of interest.

Funding

This study was supported by the São Paulo Research Foundation (FAPESP, grant numbers 2012/00259-1, 2014/25927-2, 2015/22299-3 and 2018/07862-1) to carry out the experiments. Also, this study was supported by Coordenação de Aperfeiçoamento de Pessoal de Nível Superior (CAPES) scholarship, and the Conselho Nacional de Desenvolvimento Científico e Tecnológico (CNPq, number 306311/2016-0) scholarship.

Authors' contributions

CEM performed the immunohistochemistry experiments and analyzed the results. KP and TTAP helped with ischemia/reperfusion and PB protocols. PC planned experiments, analyzed the results, and wrote and edited the manuscript. All authors have read and approved the manuscript.

Acknowledgements

São Paulo Research Foundation (FAPESP) and Coordenação de Aperfeiçoamento de Pessoal de Nível Superior (CAPES), and the Conselho Nacional de Desenvolvimento Científico e Tecnológico.

References

1. Cabarrocas J, Savidge TC, Liblau RS. Role of enteric glial cells in inflammatory bowel disease. Glia. 2003;41:81–93.
2. Neunlist M, Rolli-derkinderen M, Latorre R, Van Landeghem L, Cron E, Derkinderen P, De Giorgio R. Enteric glial cells recent developments and future directions. Gastroenterology. 2014;147(6):1230–7.
3. Rühl A. Glial cells in the gut. Neurogastroenterol Motil. 2005;17:777–90.
4. Bassotti G, Villanacci V, Fisogni S, Rossi E, Baronio P, Clerici C, Maurer CA, Cathomas G, Antonelli E. Enteric glial cells and their role in gastrointestinal motor abnormalities: Introducing the neuro-gliopathies. World J Gastroenterol. 2007;13:4035–41.

5. Flamant M, Aubert P, Rolli-Derkinderen M, Bourreille A, Neunlist MR, Mahé MM, Meurette G, Marteyn B, Savidge T, Galmiche JP, Sansonetti PJ, Neunlist M. Enteric glia protect against Shigella flexneri invasion in intestinal epithelial cells: a role for S-nitrosoglutathione. Gut. 2011;60:473–83.
6. Savidge TC, Newman P, Pothoulakis C, Ruhl A, Neunlist M, Bourreille A, Hurst R, Sofroniew MV. Enteric glia regulate intestinal barrier function and inflammation via release of S-nitrosoglutathione. Gastroenterology. 2007;132:1344–58.
7. Ferri G, Probert L, Cocchia D, Michetti F, Marangos P, Polak J. Evidence for the presence of S-100 protein in the glial component of the human enteric nervous system. Nature. 1982;297:409–10.
8. Jessen K, Mirsky R. Glial cells in the enteric nervous system contain glial fibrillary acidic protein. Nature. 1980;286:736–7.
9. Gulbransen BD, Sharkey KA. Novel functional roles for enteric glia in the gastrointestinal tract. Nat Rev Gastroenterol Hepatol. 2012;9(110):625–32.
10. Furness JB. The Enteric Nervous System. Australia: Blackwell Publishing; 2006.
11. D'hondt C, Ponsaerts R, De Smedt H, Bultynck G. Himpens B. Pannexins. distant relatives of. the connexin family with specific cellular functions? BioEssays. 2009;31:953–74.
12. Makarenkova H, Shestopalov V. The role of pannexin hemichannels in inflammation and regeneration. Front Physiol. 2014;25:5:63.
13. Panchin Y, Kelmanson I, Matz M, Lukyanov K, Usman N, Lukyanov S. A ubiquitous family of putative gap junction molecules. Curr Biol. 2000;10:R473–4.
14. Velasquez S, Eugenin E. Role of Pannexin-1 hemichannels and purinergic receptors in the pathogenesis of human diseases. Front Physiol. 2014;14(5):96.
15. Chekeni FB, Elliott MR, Sandilos JK, Walk SF, Kinchen JM, Lazarowski ER, Armstrong AJ, Penuela S, Laird DW, Salvesen GS, Isakson BEB, Ravichandran DA. KS. Pannexin 1 channels mediate 'find-me' signal release and membrane permeability during apoptosis. Nature. 2010;467:863–7.
16. Jiang JX, Peñuela S. Connexin and pannexin channels in cancer. BMC Cell Biol. 2016;17(Suppl 1):12.
17. Penuela S, Bhalla R, Nag K, Laird D. Glycosylation regulates pannexin intermixing and cellular localization. Mol Biol Cell. 2009;20:4313–23.
18. Pelegrin P, Surprenant A. Pannexin-1 mediates large pore formation and interleukin-1beta release by the ATP-gated P2X7 receptor. EMBO J. 2006;25:5071–82.
19. Diezmos EF, Markus I, Perera DS, Gan S, Zhang L, Sandow SL, Bertrand PPL, Liu L. Blockade of Pannexin-1 Channels and Purinergic P2X7 Receptors Shows Protective Effects Against Cytokines-Induced Colitis of Human Colonic Mucosa. Front Pharmacol. 2018;9:865.
20. Diezmos EF, Sandow SL, Markus I, Shevy Perera D, Lubowski DZ, King DW, Bertrand PP, Liu L. Expression and localization of pannexin-1 hemichannels in human colon in health and disease. Neurogastroenterol Motil. 2013;25:e395–405.
21. Silverman W, Locovei S, Dahl G. Probenecid, a gout remedy, inhibits pannexin 1 channels. Am J Physiol Cell Physiol. 2008;295:C761–7.

22. Bargiotas P, Krenz A, Hormuzdi SG, Ridder DA, Herb A, Barakat W, Penuela S, von Engelhardt J, Monyer H. M. S. Pannexins in ischemia-induced neurodegeneration. Proc Natl Acad Sci USA. 2011;108:20772–7.
23. Wei R, Wang J, Xu Y, Yin B, He F, Du Y, Peng G, Luo B. Probenecid protects against cerebral ischemia/reperfusion injury. by inhibiting lysosonal and inflammatory damage in rats. Neuroscience. 2015;301:168–77.
24. Vollmar B, Menger MD. Intestinal ischemia/reperfusion: microcirculatory pathology and functional consequences. Langenbecks Arch Surg. 2011;396:13–29.
25. Maes M, Cogliati B, Crespo YS, Willebrords J, Vinken M. Roles of connexins and pannexins in digestive homeostasis. Cell Mol Life Sci. 2015;72:2809–21. doi:10.1007/s00018-015-1961-8.
26. McClain JL, Grubišić V, Fried D, Gomez-Suarez RA, Leinninger GM, Sévigny J, Parpura V, Gulbransen BD. Ca2 + responses in enteric glia are mediated by connexin-43 hemichannels and modulate colonic transit in mice. Gastroenterology. 2014;146(2):497–507. doi:10.1053/j.gastro. 2013.10.061. [PubMed: 24211490].
27. Vieira C, Ferreirinha F, Magalhães-Cardoso MT, Silva I, Marques P, Correia-de-Sá P. Post-inflammatory Ileitis Induces Non-neuronal Purinergic Signaling Adjustments of Cholinergic Neurotransmission in the Myenteric Plexus. Front Pharmacol. (2017) 8:811. https://doi.org/10.3389/fphar.2017.00811.
28. Gulbransen BD, Bashashati M, Hirota SA, Gui XY, Roberts JA, MacDonald JA, Muruve DA, McKay DM, Beck PL, Mawe GM, Thompson RJ, Sharkey KA. Activation of neuronal P2X7 receptor-pannexin-1 mediates death of enteric neurons during colitis. Nat Med. 2012;18:600–4.
29. Mendes CE, Palombit K, Vieira C, Silva I, Correia-de-Sá P, Castelucci P. The Effect of Ischemia and Reperfusion on Enteric Glial Cells and Contractile Activity in the Ileum. Dig Dis Sci. 2015;60:2677–89.
30. Mendes C, Palombit K, Tavares-de-Lima W, Castelucci P. Enteric glial cells immunoreactive. for P2X7 receptor are affected in the ileum following ischemia and reperfusion. Acta Histochem. 2019;121:665–679.
31. Palombit K, Mendes CE, Tavares-de-Lima W, Barreto-Chaves ML, Castelucci P. Blockage of the P2X7 Receptor Attenuates Harmful Changes Produced by Ischemia and Reperfusion in the Myenteric Plexus. Dig Dis Sci. 2019;64:1815–29.
32. Palombit K, Mendes CE, Tavares-de-Lima W, Silveira MP, Castelucci P. Effects of Ischemia and Reperfusion on Subpopulations of Rat Enteric Neurons Expressing the P2X7 Receptor. Dig Dis Sci. 2013;58:3429–39.
33. Locovei S, Scemes E, Qiu F, Spray DC, Dahl G. Pannexin1 is part of the pore forming unit of. the P2X(7) receptor death complex. FEBS Lett. 2007;581:483–8.
34. Locovei S, Wang J, Dahl G. Activation of pannexin 1 channels by ATP through P2Y receptors and by cytoplasmic calcium. FEBS Lett. 2006;80:239–44.
35. Xia J, Lim JC, Lu W, Beckel JM, Macarak EJ, Laties AM, Mitchell CH. Neurons respond directly to mechanical deformation with pannexin-mediated ATP release and autostimulation of P2X7 receptors. J Physiol. 2012;590:2285–304.

36. Boesmans W, Lasrado R, Vanden Berghe P, Pachnis V. Heterogeneity and phenotypic plasticity of glial cells in the mammalian enteric nervous system. Glia. 2015;63:229–41.
37. Grundmann D, Markwart F, Scheller A, Kirchhoff F, Schäfer KH. Phenotype and distribution pattern of nestin-GFP- expressing cells in murine myenteric plexus. Cell Tissue. Res. 2016;366:573–86.
38. Grundmann D, Loris E, Maas-Omlor S, Huang W, Kirchhoff AS, Schäfer F, Enteric Glia K. S100, GFAP, and Beyond. Anat Rec (Hoboken). 2019;302:1333–44.
39. Jian Z, Ding S, Deng H, Wang J, Yi W, Wang L, Zhu S, Gu L, Xiong X. Probenecid protects against oxygen-glucose deprivation injury in primary astrocytes by regulating inflammasome activity. Brain Res. 2016;1643:123–9.
40. Xiong XX, Gu LJ, Shen J, Kang XH, Zheng YY, Yue SB, Zhu SM. Probenecid protects against transient focal cerebral ischemic injury by inhibiting HMGB1 release and attenuating AQP4 expression in mice. Neurochem Res. 2014;39:216–24.
41. Donato R. Intracellular and extracelular roles of S100 proteins. Microsc Res Tech. 2003;60:1008–22.
42. Donato R, Sorci G, Riuzzi F, Arcuri C, Brozzi RB, Tubaro F, Giambanco C. I. S100B's double life: intracellular regulator and extracellular signal. Biochim Biophys Acta. 2009;1793:1008–22.
43. Vanden Abeele F, Bidaux G, Gordienko D, Beck B, Panchin YV, Baranova AV, Ivanov DV, Skryma R, Prevarskaya N. Functional implications of calcium permeability of the channel formed by pannexin 1. J Cell Biol. 2006;174:535–46.
44. Cisneros-Mejorado A, Gottlieb M, Cavaliere F, Magnus T, Koch-Nolte F, Scemes E, Pérez-Samartín A, Matute C. Blockade of P2X7 receptors or pannexin-1 channels similarly attenuates post ischemia damage. J Cereb Blood Flow Metab. 2015;35:843–50.
45. Bhaskaracharya A, Dao-Ung P, Jalilian I, Spildrejorde M, Skarratt KK, Fuller SJ, Sluyter R, Stokes L. L. Probenecid blocks human P2X7 receptor-induced dye uptake via a pannexin-1 independent mechanism. PLoS ONE. 2014;26:e93058.
46. Rivera LR, Pontell L, Cho H-J, Castelucci P, Thacker M, Poole DP, Frugier T, Furness JB. Knock out of neuronal nitric oxide synthase exacerbates intestinal ischemia/reperfusion injury in mice. Cell Tissue Res. 2012;349:565–76.
47. Ballabeni V, Barocelli E, Bertoni S, Impicciatore M. Alterations of intestinal motor responsiveness in a model of mild mesenteric ischemia/reperfusion in rats. Life Sci. 2002;71:2025–35.
48. Burnstock G, Jacobson K, Christofi F. Purinergic drug targets for gastrointestinal disorders. Curr Opin Pharmacol. 2017;37:131–41.
49. Ren J, Bertrand P. Purinergic receptors and synaptic transmission in enteric neurons. Purinergic Signal. 2008;4:255–66.
50. Galligan JJ, North RA. Pharmacology and function of nicotinic acetylcholine and P2X receptors in the enteric nervous system. Neurogastro Mot. 2004;16:64–70.
51. Aube AC, Cabarrocas J, Bauer J, Philippe D, Aubert P, Doulay F, Liblau R, Galmiche JP. Neunlist, M. Changes in enteric neurone phenotype and intestinal functions in a transgenic mouse model of

enteric glia disruption. Gut. 2006;55:630–7.

52. Nasser Y, Fernandez E, Keenan CM, Ho W, Oland LD, Tibbles LA, Schemann M, MacNaughton WK, Rühl A, Sharkey KA. Role of enteric glia in intestinal physiology: effects of the gliotoxin fluorocitrate on motor and secretory function. Am J Physiol Gastrointest Liver Physiol. 2006;291:G912–27.

Figures

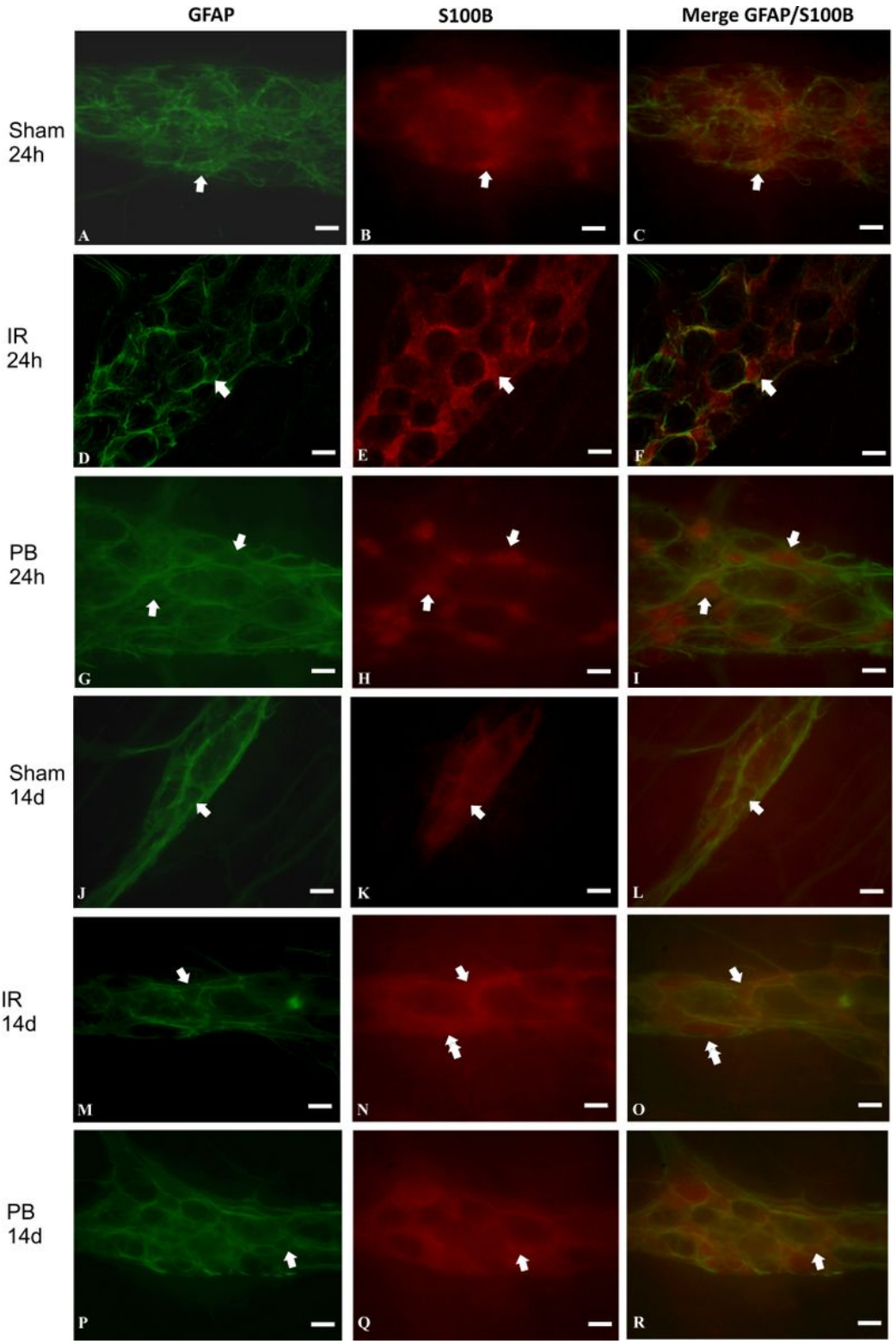

Figure 1

Double labeling of GFAP and S100β in the rat ileum myenteric plexus of the Sh (A-C; J-L), IR (D-F; M-O) and PB (G-I; P-R) groups at 24 h (A-I) and 14 days (J-R). GFAP (*green*; A, D, G, J, M, P) colocalized with S100β (*red*; B, E, H, K, N, Q). Merge GFAP (green) with S100B (red) (C-R). Single arrows indicate double-labeled EGCs. The double arrows indicate no colocalization. Scale bars, 10 μm. The preparations were examined with a Nikon 80i fluorescence microscope and by confocal microscopy using a Zeiss confocal scanning laser system installed on a Zeiss Axioplan 2 microscope.

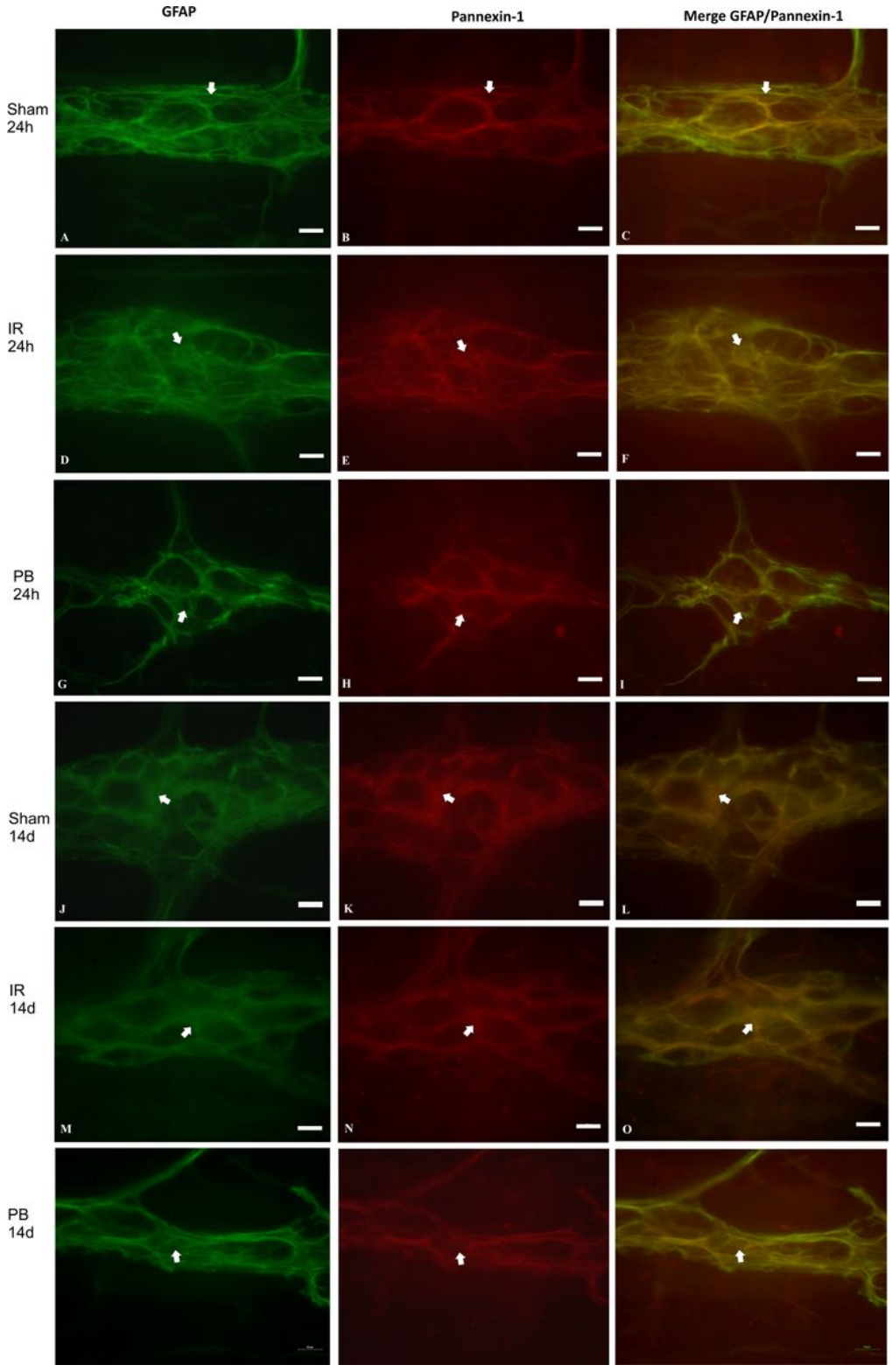

Figure 2

Double labeling of GFAP and Pannexin-1 in the rat ileum myenteric plexus of the Sh (A-C; J-L), IR (D-F; M-O) and PB (G-I; P-R) groups at 24 h (A-I) and 14 days (J-R). GFAP (*green*; A, D, G, J, M, P) colocalized with Pannexin-1 (*red*; B, E, H, K, N, Q). Merge GFAP (green) with S100B (red) (C-R). Single arrows indicate double-labeled EGCs. Scale bars, 10 μm. The preparations were examined with a Nikon 80i fluorescence

microscope and by confocal microscopy using a Zeiss confocal scanning laser system installed on a Zeiss Axioplan 2 microscope.

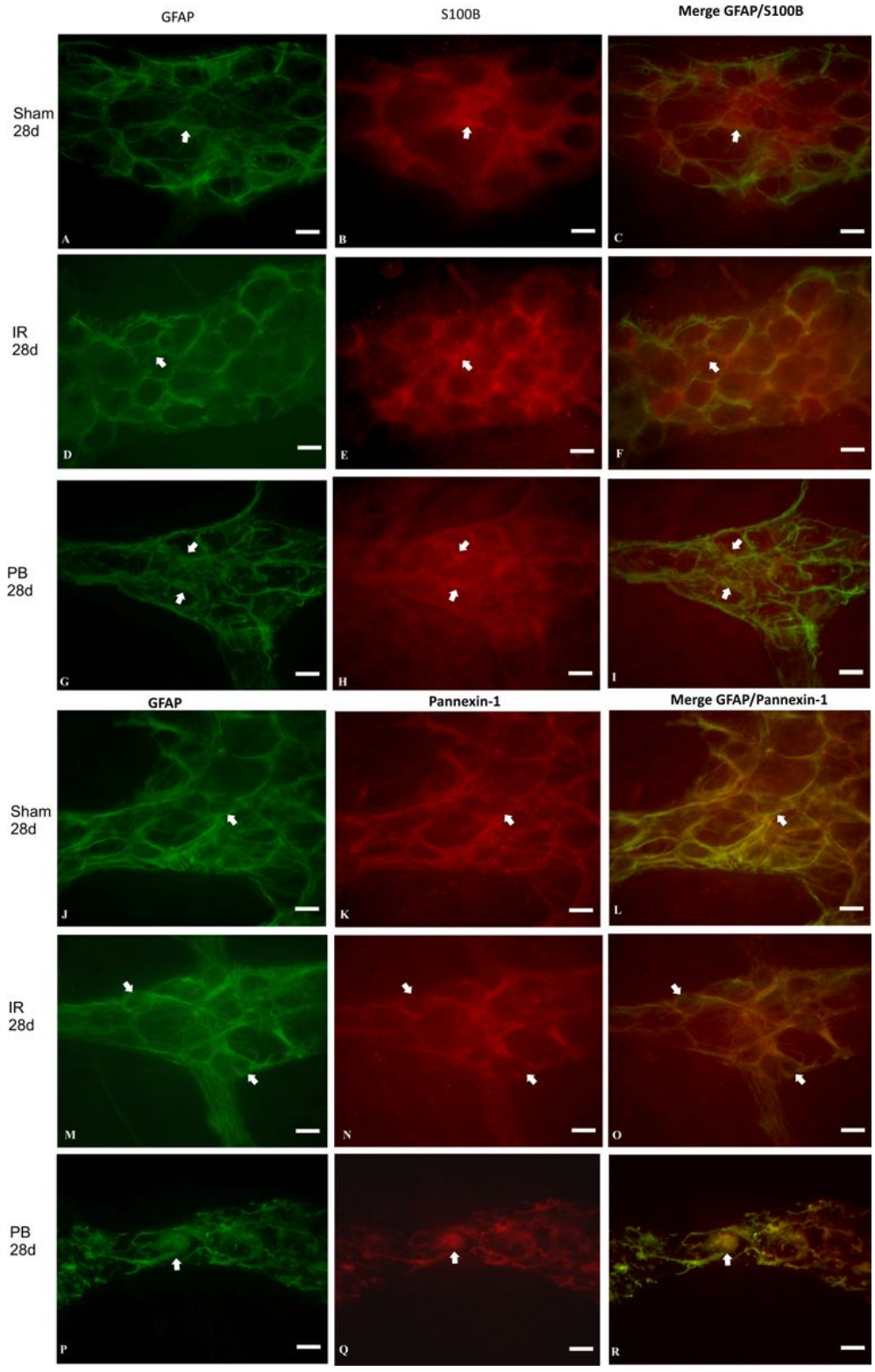

Figure 3

Double labeling of GFAP and S100B (A-I), GFAP and Pannexin-1 (J-R) in the rat ileum myenteric plexus of the Sh (A-C; J-L), IR (D-F; M-O) and PB (G-I; P-R) groups at 28 days. GFAP (*green*; A, D, G) colocalized with

S100B (*red*; B, E, H). GFAP (*green*; J, M, P) colocalized with Pannexin-1 (*red*; K, N, Q). Merge GFAP (green) with S100B (red) (C-I). Merge GFAP (green) with Pannexin-1 (red) (L-R). Single arrows indicate double-labeled EGCs. Scale bars, 10 μm. The preparations were examined with a Nikon 80i fluorescence microscope and by confocal microscopy using a Zeiss confocal scanning laser system installed on a Zeiss Axioplan 2 microscope.

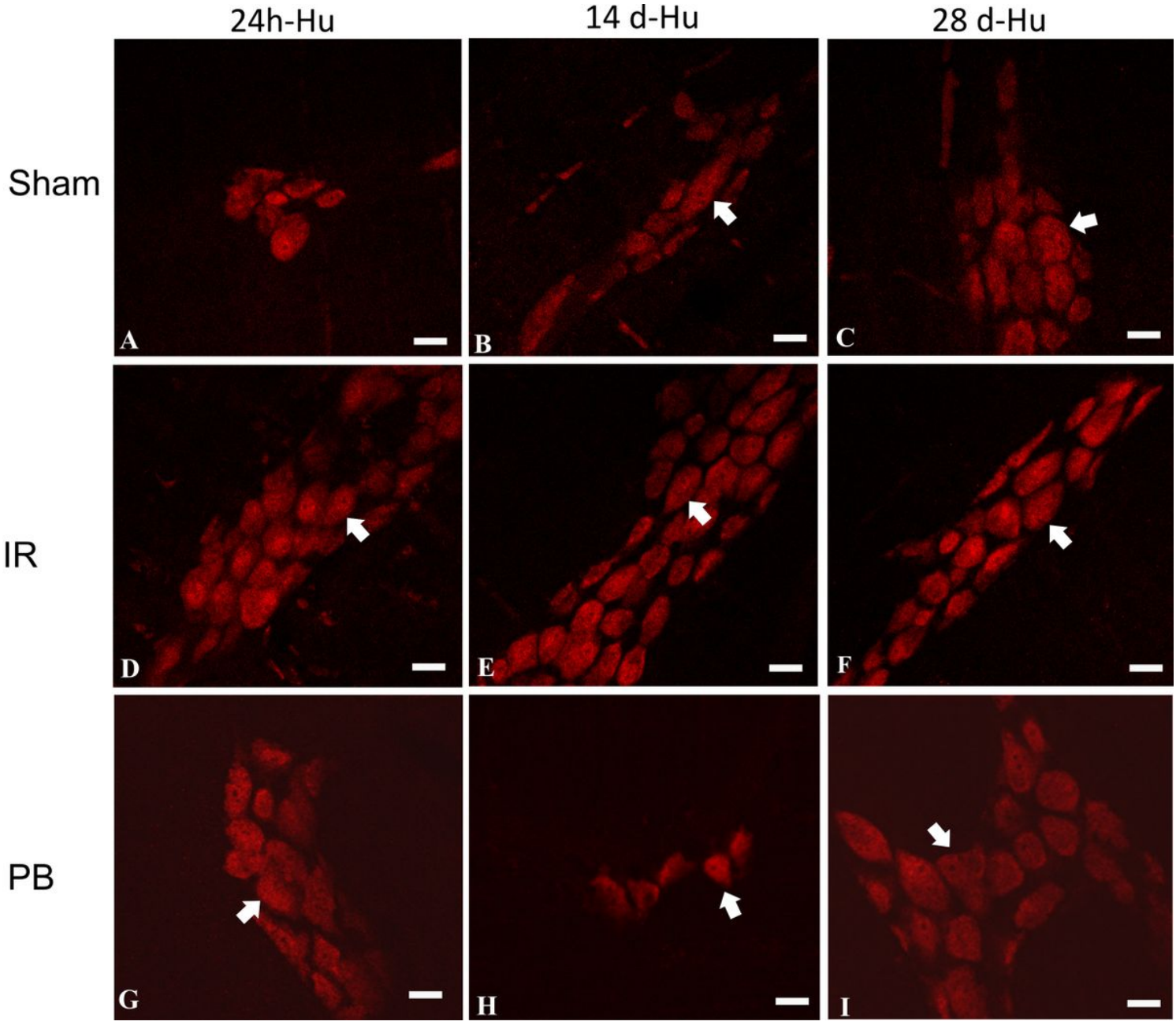

Figure 4

Labeling of HuC/D (Hu, pan neuronal) in the rat ileum myenteric plexus of the Sh (A-C), IR (D-F) and PB (G-I) groups at 24 h, 14 days and 28 days. Single arrows indicate label neurons positive for HuC/D. Scale bars, 20 μm. The preparations were examined with a Nikon 80i fluorescence microscope and by confocal microscopy using a Zeiss confocal scanning laser system installed on a Zeiss Axioplan 2 microscope.

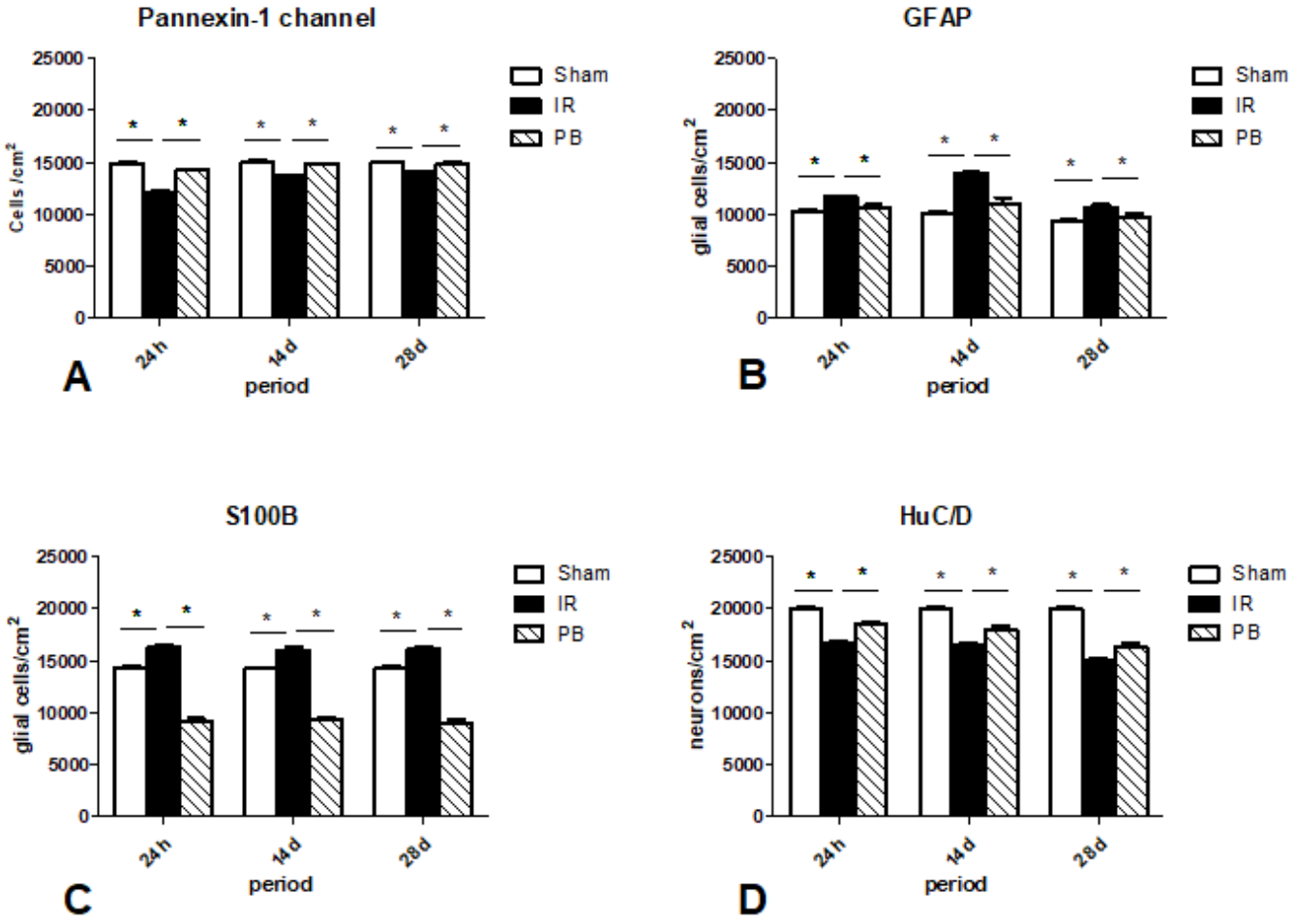

Figure 5

Neurons immunoreactive for the pannexin-1 channel (A), GFAP (B), S100β (C) and HuC/D (D) per unit area in the ileum myenteric plexus of the Sh, IR and PB groups at 24 h, 14 days and 28 days. For each antigen, counts were obtained from 40 microscopic fields (0.000379 cm^2) selected at random in two whole-mount preparations per animal, and five rats from each group were included in the analysis (45 rats total). Each column represents pooled data from five individual immunofluorescence experiments. The data are presented as the means ± SEMs (n=5 per group) and were compared by one-way ANOVA and Tukey's multiple comparison test (*$P < 0.05$ and **$P < 0.01$). The preparations were examined with a Nikon 80i fluorescence microscope.

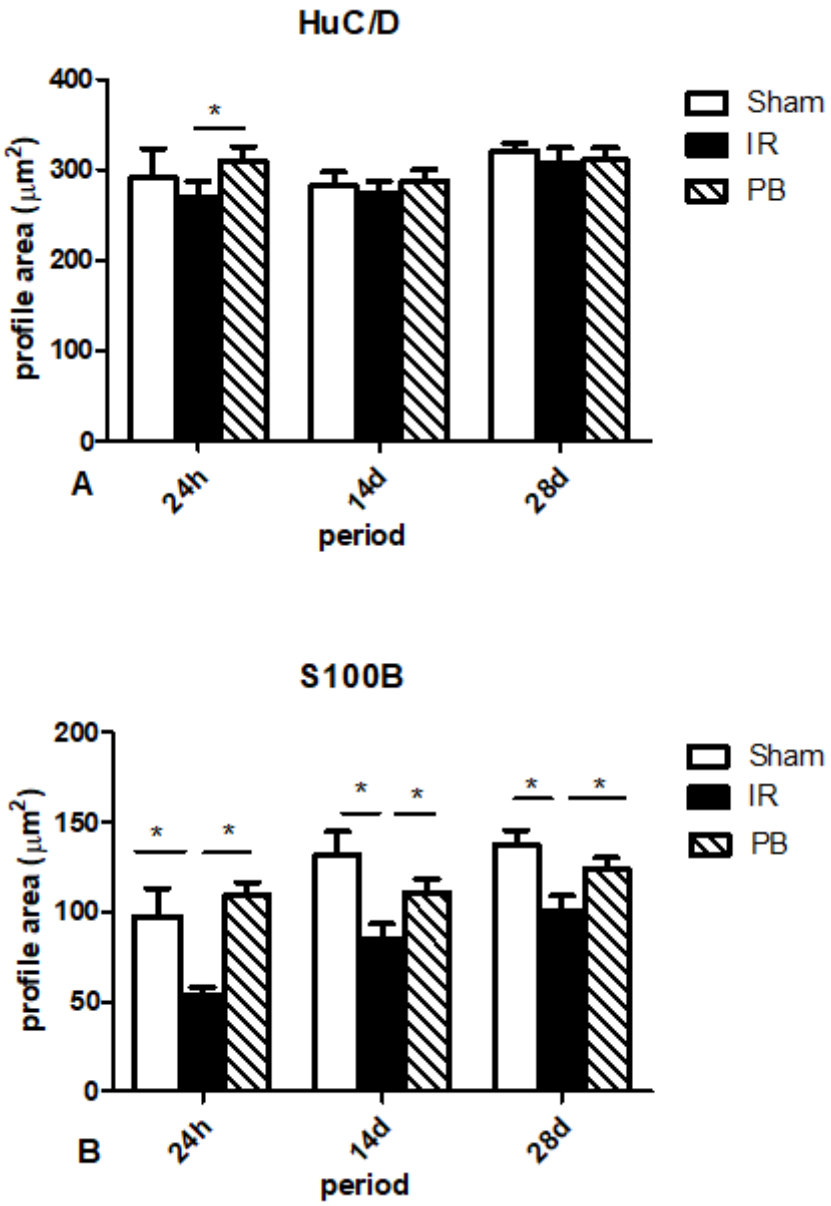

Figure 6

Profile areas (μm^2) of the of neurons positive for HuC/D (A) and S100β (B) and in the ileum myenteric plexus of the Sh, IR and PB groups at 24 h, 14 days and 28 days. The cell profile areas (μm^2) were obtained for 100 randomly selected neurons in two whole-mount preparations per animal, and five rats from each group (45 rats total) were used in each immunoreactivity assay. Each column represents pooled data from 500 neurons. The data are presented as the means ± SEMs and were compared by one-way ANOVA and Tukey's multiple comparison test (*$P < 0.05$ and **$P < 0.01$). The preparations were examined with a Nikon 80i fluorescence microscope.

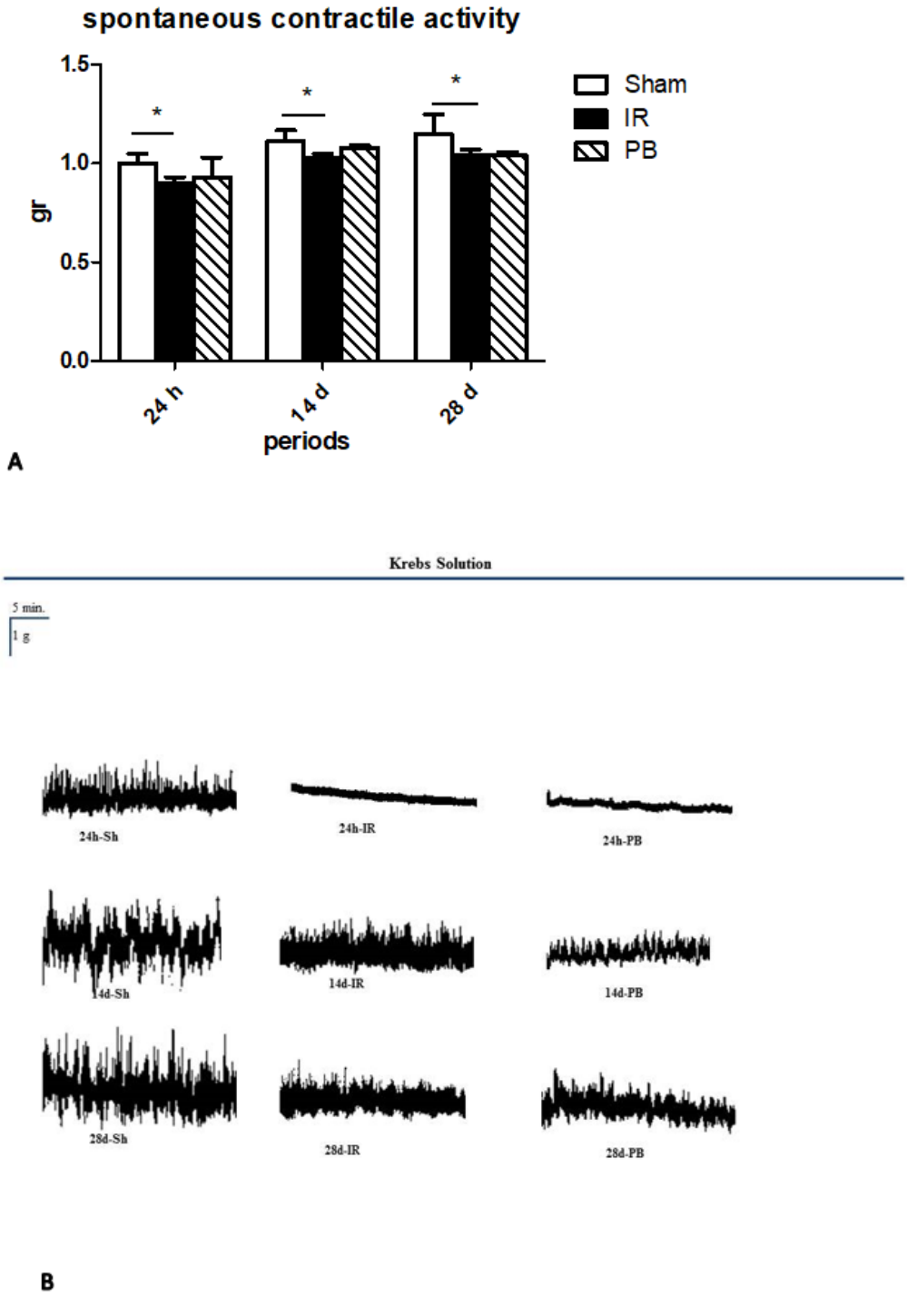

Figure 7

Contractile activity of ileal segments from Sh, IR and PB groups at 24 h, 14 days and 28 days. Changes in the amplitude of spontaneous activity following the different treatments (A). Traces showing spontaneous contractions of the ileum (B). Full-thickness ileal segments from four rats in each group were prepared and quantitatively analyzed. A total of 36 rats were used, and a total of 36 segments were analyzed. Each column represents pooled data from four individual experiments. The data are shown as

the means ± SEMs and were compared by one-way ANOVA and Tukey's multiple comparison test (*P < 0.05).

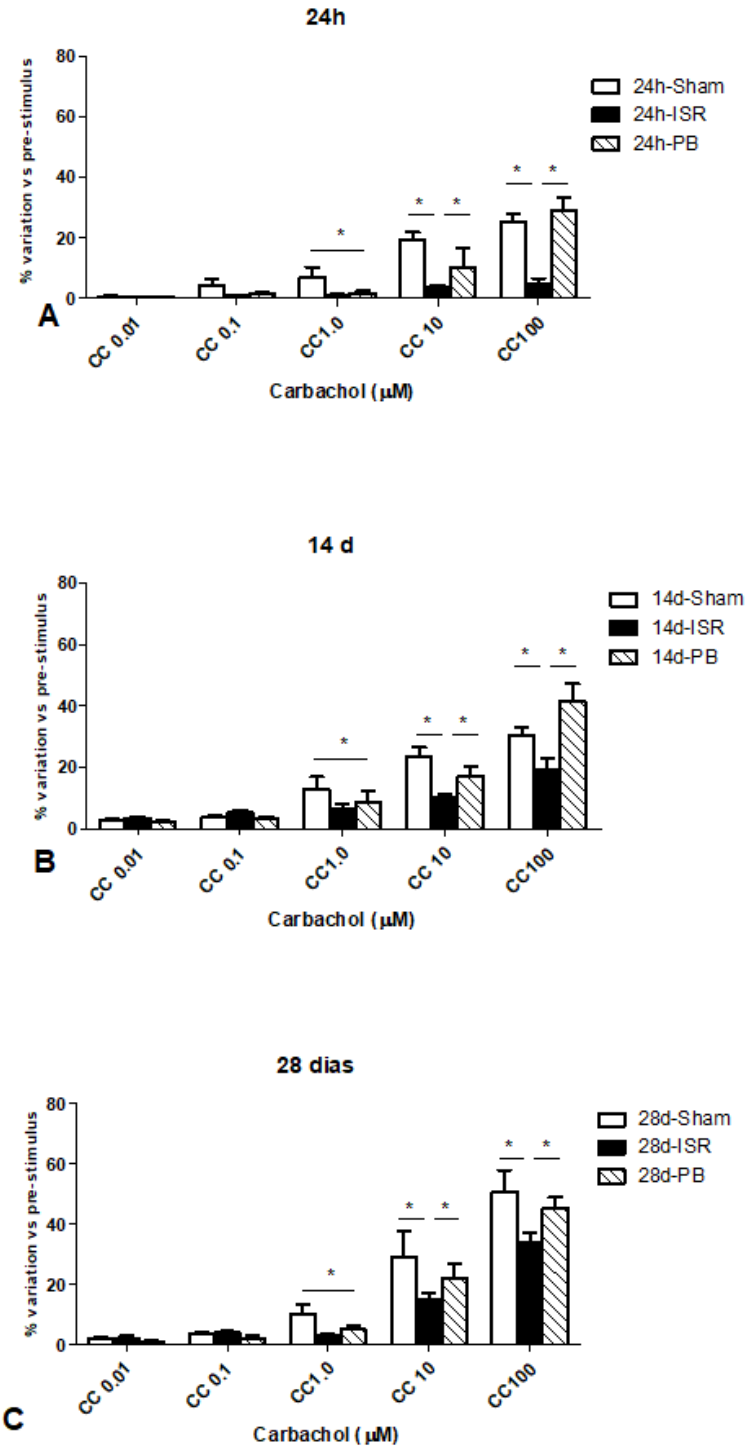

Figure 8

Contractile activity of ileal segments of the Sh, IR and PB groups at 24 h, 14 days and 28 days. Amplitude of response to carbachol at 24 h (A), 14 days (B) and 28 days (C) in groups that had received different

treatments. Traces showing the contractions elicited in response to 0.01 μM, 0.1 μM, 1.0 μM, 10 μM and 100 μM carbachol at the different periods (D). Full-thickness ileal segments from four rats in each group were prepared and analyzed. A total of 36 rats were used, and a total of 36 segments were analyzed. Each column represents pooled data from five individual experiments. The data are shown as the means ± SEMs and were compared by one-way ANOVA and Tukey's multiple comparison test (*$P < 0.05$).

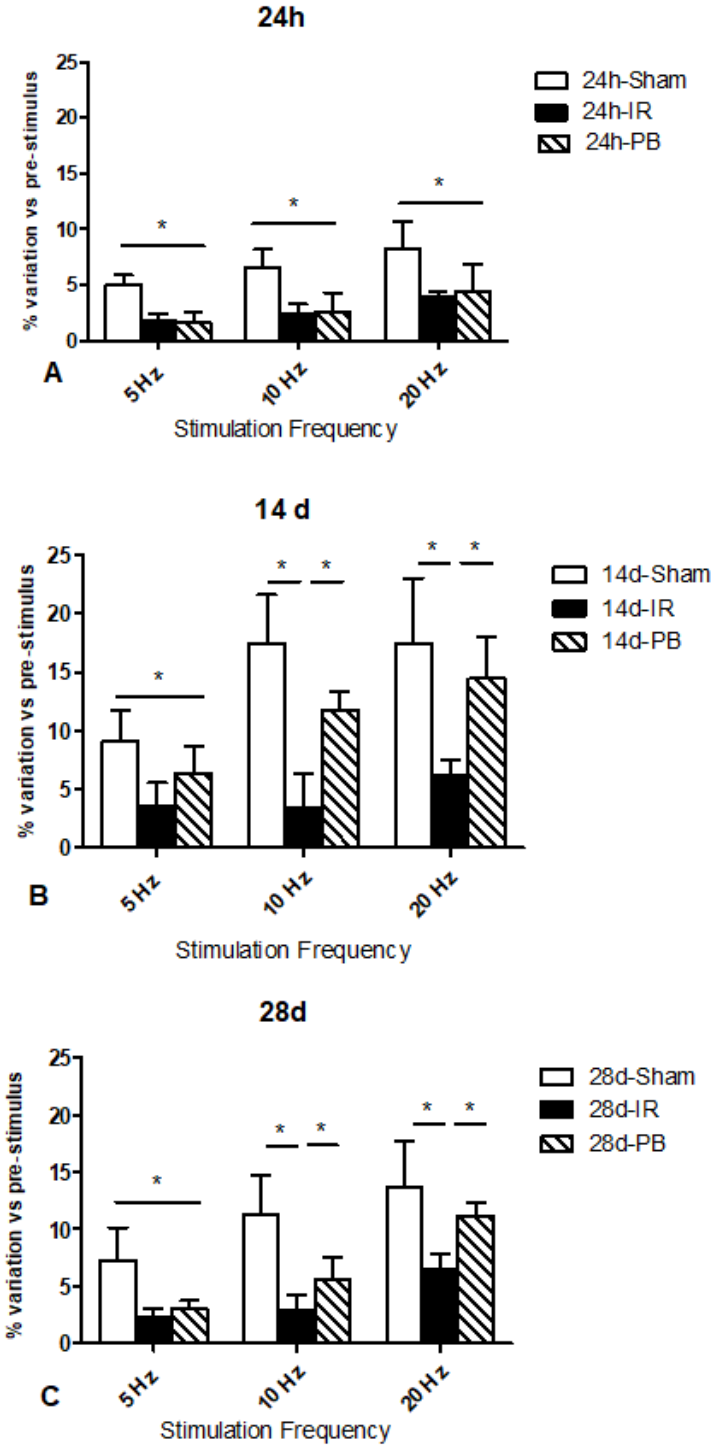

Figure 9

Contractile activity of ileal segments of the Sh, IR and PB groups at 24 h, 14 days and 28 days. Amplitude in response to electrical field stimulation at 24 h (A), 14 days (B) and 28 days (C) in groups that had received different treatments. Tracings showing the contractions elicited by 5-, 10- and 20-Hz electrical field stimulation (D). Full-thickness ileal segments from four rats in each group were prepared and analyzed. A total of 36 rats were used, and a total of 36 segments were analyzed. Each column represents pooled data from five individual experiments. The data are shown as the means ± SEMs and were compared by one-way ANOVA and Tukey's multiple comparison test (*$P < 0.05$).

Supplementary Files

This is a list of supplementary files associated with this preprint. Click to download.

- ARRIVEguidelines2.0English.pdf